

THREE DIMENSIONAL MODELING OF RELATIVISTIC COLLISIONLESS ION-ELECTRON SHOCKS

TROELS HAUGBØLLE
Niels Bohr Institute
Submitted to ApJ Letters

ABSTRACT

Two dimensional modeling of collisionless shocks has been of tremendous importance in understanding the physics of the non-linear evolution, momentum transfer and particle acceleration, but current computer capacities have now reached a point where three dimensional modeling is becoming feasible. We present the first three dimensional model of a fully developed and relaxed relativistic ion-electron shock, and analyze and compare it to similar 2D models. Quantitative and qualitative differences are found with respect to the two-dimensional models. The shock jump conditions are of course different, because of the extra degree of freedom, but in addition it is found that strong parallel electric fields develop at the shock interface, the level of magnetic field energy is lower, and the non-thermal particle distribution is shallower with a powerlaw index of ~ 2.2 .

Subject headings: acceleration of particles — instabilities — magnetic fields — plasmas — shock waves

In collisionless shocks the mean free path of individual particles is much larger than the characteristic scales in the shock structure, and effective collisions and pressure support are not mediated in particle-particle interactions, but by collective forces. Collisionless shocks are ubiquitous in the universe, and happen on a range of scales from the bow-shock of the solar wind at the earth, over solar corona, supernova remnants to highly relativistic shocks at gamma-ray bursts and active galactic nuclei. Given that only collective forces act as an effective collision mechanism, instabilities can easily arise in the plasma. It has been shown over the last ten years how a range of Weibel-like filamentation instabilities operate at the shock interface (Kazimura et al. 1998; Medvedev & Loeb 1999; Bret et al. 2004; Frederiksen et al. 2004; Silva et al. 2003; Nishikawa et al. 2003; Keshet et al. 2009), which can lead to magnetic field generation and particle acceleration. A breakthrough for the study and understanding of collisionless shocks has been the application of *ab initio* particle-in-cell simulations, where the formation and evolution beyond the linear phase of the instabilities of the shocks can be studied with almost no assumptions. Until now, the largest scale computer experiments of both magnetized (Shimada & Hoshino 2004; Saito & Sakai 2004; Hededal & Nishikawa 2005; Spitkovsky 2005; Sironi & Spitkovsky 2009) and unmagnetized (Haugbølle 2005; Hededal 2005; Spitkovsky 2005; Silva 2006; Kato 2007; Chang et al. 2008; Spitkovsky 2008a,b; Martins et al. 2009) collisionless shocks have mostly been performed in two dimensions, while three dimensional simulations of unmagnetized shocks have been too costly to scale to large enough sizes. Some of the first studies of electron-positron and electron-ion shocks were performed in 3D, but only the very early linear and quasi-linear stages of the shock formation could be followed (Frederiksen et al. 2004; Silva et al. 2003; Nishikawa et al. 2003). Three dimensional studies of pair plasmas have been done showing the full development of the shock ramp, and recovering the correct jump conditions (Haugbølle 2005; Spitkovsky 2005; Nishikawa et al. 2009), but only limited electron-ion simulations have been made (Spitkovsky 2008a).

The development of long term large scale two dimensional simulations have helped tremendously in the understanding

of collisionless shocks, both in quantitative and qualitative terms, but given current computational resources, and the technical quality of the Particle-In-Cell codes, we now have the possibility of using fully three dimensional modeling to properly account for the full dynamics. In this paper we present the first three dimensional simulation of a relativistic unmagnetized collisionless electron-ion shock, where the simulation is followed long enough to establish the correct jump conditions, create a fully thermalized and developed downstream region, and follow the emergence of a power-law distributed population of high energy ions and electrons downstream of the shock. We compare the results to similar 2D simulations, and show how the different dimensionality impacts on the formation and evolution of the shock.

1. SIMULATION SETUP

We have used the massively parallel 3D particle-in-cell *Photon-Plasma* code, developed at the Niels Bohr Institute (Haugbølle 2005; Hededal 2005), to simulate collisionless electron-ion shocks. For the three dimensional ion-electron run we used a 2nd order field solver and TSC interpolation of particles, while for all other runs we used a newly developed 6th order field solver and cubic interpolation of particles, giving effectively a 50% higher resolution (see e.g. PCCP). The simulation domain is periodic perpendicular to the streaming direction, while the lower inflow boundary is open for outgoing particles and has absorbing field boundaries and the opposite, upper boundary is a perfectly reflecting wall. We use a combination of a moving injector, to launch the shock (Sironi & Spitkovsky 2009), and a moving window, to follow the shock evolution (Tzeng et al. 1996). Initially, only a small slice in front of the wall is populated with a streaming plasma, and a shock is launched when the reflected fields and particles collide with the inflowing plasma. New particles are added to the plasma in front of the shock with the speed of light until the full box is populated with a streaming plasma. At the lower boundary outgoing particles are allowed to escape the box, and electromagnetic fields are damped while the shock transition propagates through the box and the downstream region grows. When the shock transition reaches the center of the box, a moving frame is applied which continuously moves the simulation domain to keep the shock transition at the center. Initially the plasma is unmagnetized, and hence

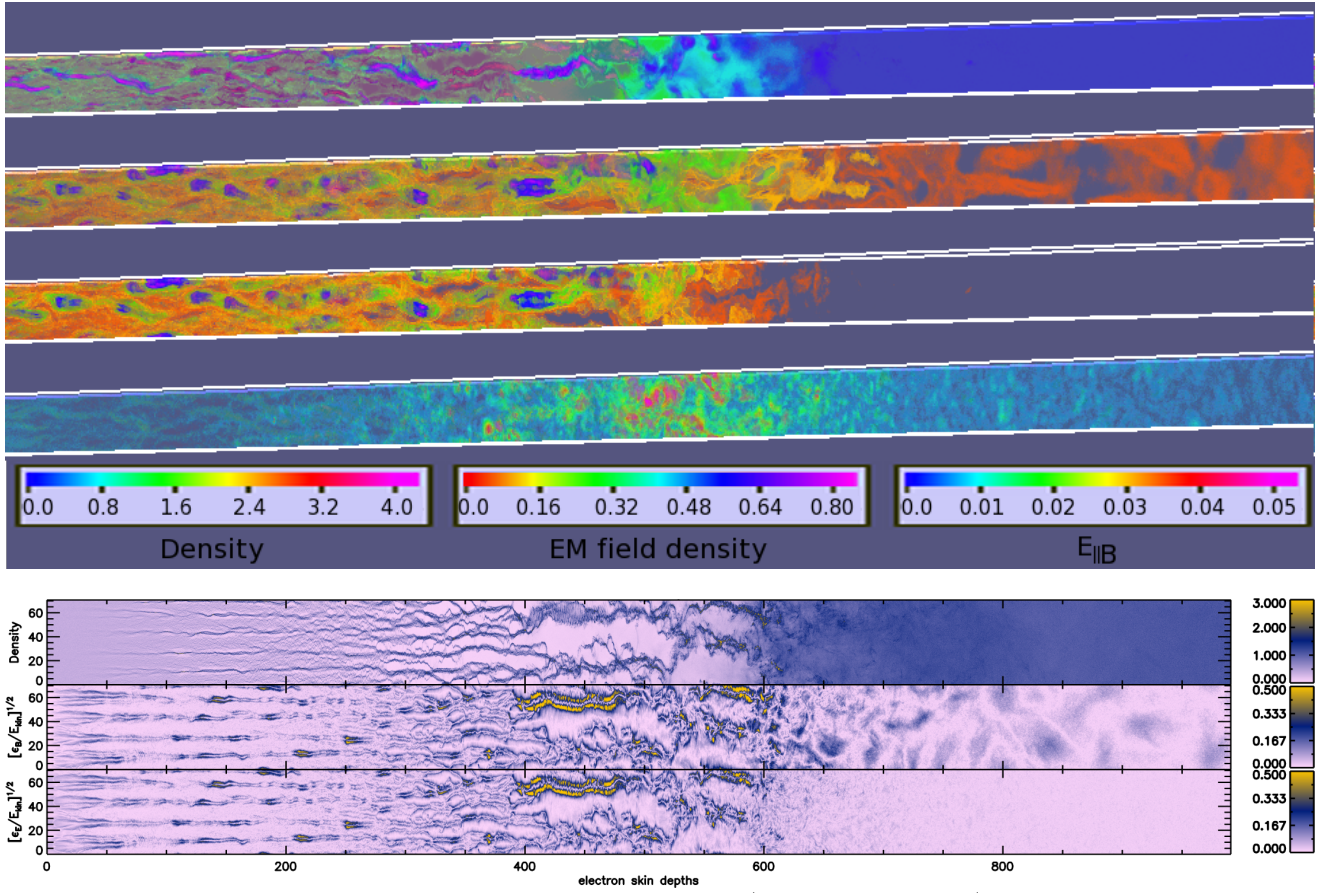


FIG. 1.— Upper panel: From top to bottom the ion density, the magnetic field density $\epsilon_B^{1/2}$, electric field density $\epsilon_E^{1/2}$, and the electric field projected along the magnetic field lines $E_{\parallel B}$ at $\omega_{pe} t = 2250$. The fields are normalized to the kinetic energy density of the upstream bulk flow, as for example $\epsilon_B = B^2 / [2n(m_i + m_e)(\Gamma - 1)]$. Lower panel: From top to bottom the ion density (normalized to 1/3 upstream), the magnetic field density, and the electric field density at $\omega_{pe} t = 1500$ for a 2D collisionless shock.

nearly transparent for the particles. The particles reflected by the wall creates an artificial counter-streaming population of particles upstream of the shock transition region. While in 2D simulations the domain can be made large enough for this initial spike of particles to diminish in density and become insignificant, the required domain sizes are currently prohibitively expensive in 3D. But with the combination of the open lower boundary and the moving frame technique we can nevertheless follow the evolution of the shock until it has settled to a steady state, with a thermalized population downstream of the shock, and an in-streaming population mixed with particles reflected from the shock upstream. All runs have been done with an upstream Lorentz factor of $\Gamma = 15$. The 3D simulation was done with $250 \times 250 \times 7000$ cells, 6 particles per species per cell, a mass ratio m_i/m_e of 16, and contained up to 16 billion particles. To properly resolve the dynamics both up- and downstream of the shock we resolve the electron skin depth $\delta_e = (4\pi n_e e^2 / m_e \Gamma)^{1/2}$ with 14 grid cells upstream and 7 cells downstream of the shock, corresponding to 56 and 23 cells per ion skin depth up- and downstream of the shock. For the time stepping we used a Courant condition of 0.4, checking both light crossing time in a grid cell, and the local plasma frequency. To check the impact the box size had on the evolution we ran 2D simulations with initially 250×7000 cells and then wider and longer boxes with up to 1000×14000 cells. Additionally, to probe a larger dynamic range in 3D we also performed a pair-plasma simulation with $375 \times 375 \times 3750$ cells and 7.5 cells / skin depth, for a volume

of $50 \times 50 \times 500$ skin depths.

2. SHOCK STRUCTURE AND EVOLUTION

Figure 1 shows the structure of the evolved 3-D shock at $\omega_{pe} t = 2250$. Upstream of the shock the particles reflected at the shock interfaces interact with the incoming particles, generating a two-stream instability where the ions collect into current channels and are pinched by the self-generated magnetic field. The electrons Debye-shield the ions while oscillating in the strong transverse electric field, giving effective electron heating and momentum transfer from ions to electrons. The current channels slowly merge while losing momentum, and break up at the shock interface. The behavior of the upstream medium in the 3D simulation is in qualitative agreement with the 2D simulations, though the current channels in 3D seem to merge less than in 2D. This may be due to the fact that current channels in 2D (being 1D curves) necessarily cross, while in 3D that is not the case (compare e.g. densities in fig. 1). The average ϵ_B and the level of electron to ion momentum are similar in 2D and 3D (see figure 2), while the average ϵ_B with a maximum at 8% is slightly lower in 3D. Eventually the highly intermittent electromagnetic fields in the upstream current channels have transferred sufficient bulk flow energy to heat and transverse momentum to make the channels diffuse and slow down. A transition to a downstream shocked medium occurs over approximately 20 ion skin depths, equivalent to about one Larmor radius (given that the ions and electrons have approximately the same en-

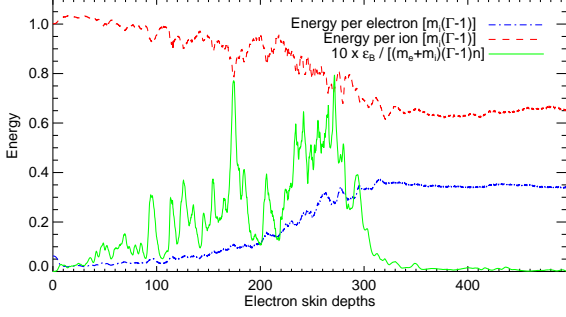


FIG. 2.— Average energy distribution across the shock at $\omega_{pe} t = 2250$. To avoid biasing only particles with positive velocities are used in calculating the average kinetic energy per particle, and the magnetic field density is normalized to the in-streaming bulk kinetic energy.

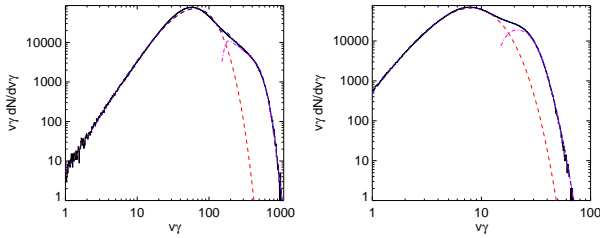


FIG. 3.— Particle distribution function sampled downstream of the shock above the dashed line marked on figure 5 at $\omega_{pe} t = 2250$. To the left are electrons and to the right ions. The red dashed line is a relativistic Maxwellian, the purple line is a powerlaw with a low and high- γ cut-off, and the blue line is the combined model.

ergy, their Larmor radii are similar). While the width of the shock transition is nearly the same in 2D and 3D, unique for 3D is the occurrence of large electric fields parallel with the magnetic field (see upper panel in figure 1) in the transition region, coupled with $\epsilon_B = 1$ locally, giving an effective mechanism for ion and electron acceleration across the shock transition. A similar phenomena has been observed with satellites in the collisionless shocks in the aurora and the Earth’s magnetosphere, where parallel electric fields together with strong particle acceleration are observed at the shock transition (see e. g. Ergun et al. 2001, 2009). We also note that parallel electric fields play a key role in reconnection of magnetic fields (Schindler et al. 1988), such as the reconfiguration that happens here, going from the mostly transverse current driven axial magnetic field upstream of the shock to the turbulent flux ropes seen downstream of the shock. In the downstream region the plasma is very nearly neutral, with little density variation, but with a high level of magnetic turbulence. Our current simulation box for the ion-electron shock is not wide enough to allow for the largest magnetic structures, but using a 3D pair plasma simulation with a larger transverse volume we have observed how closed flux ropes are formed and are advected downwards from the shock, similar to what was seen by Spitkovsky (2005).

3. PARTICLE ACCELERATION AND DISTRIBUTION

In 2D models of collisionless shocks it has been found that particles are slowly accelerated by scattering off the filaments (Heddal et al. 2004; Spitkovsky 2008b; Martins et al. 2009). A few “lucky” particles cross back and forth over the shock interfaces a number of times, and this Fermi-like acceleration process slowly builds up a power-law tail of high energy particles, due to the quasi constant probability that a single

high-energy particle is reflected in the strong transverse electric field near the shock (Martins et al. 2009). Even though the acceleration mechanism is not identical to the normal Fermi process, the resulting power-law index is in good agreement with theoretical predictions, and is approximately $\alpha = 2.3 - 2.6$, where $f(p) \propto \gamma^{-\alpha}$ at high energies. In our 3D simulation we find the same emergence of a high energy tail distribution, on top of a relativistic Maxwellian downstream of the shock. We model it as

$$f(v\gamma) = A_1(v\gamma)^2 \exp(-m_{i,e}\gamma/T) + A_2\gamma^{-\alpha} [1 + \exp(-(\gamma_{min} - \gamma)/\Delta_{min})]^{-1} [1 + \exp(-(\gamma - \gamma_{max})/\Delta_{max})]^{-1} \quad (1)$$

where A_i are normalizations, T is the temperature, α is the powerlaw slope, and γ_i & Δ_i are the locations and widths of the cut-offs. We impose the low energy cut-off so the powerlaw makes a smooth match to the Maxwellian, while the upper cut-off is time-dependent and grows with time. We find that in the 3D simulation the slope is shallower with $\alpha = 2.1 - 2.3$, matching the theoretical prediction of Keshet & Waxman (2005), for a $\Gamma = 15$ relativistic shock of $\alpha_{theo} = 2.1$.

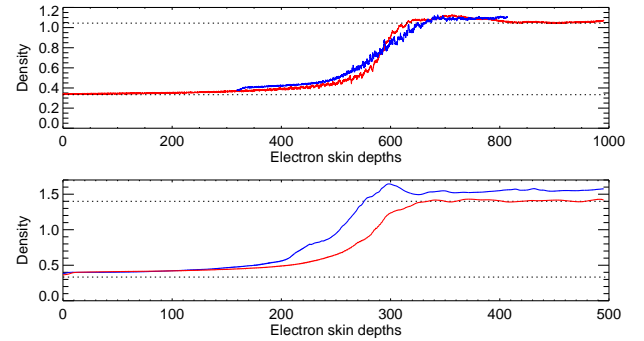


FIG. 4.— Density profile of the 2D and 3D runs. In the upper panel the density profile at $\omega_{pe} t = 1600$ is shown for a 14000x1000 cell domain, and a 7000x250 cell domain. In the lower panel the density profile for the 3D run at the times $\omega_{pe} t = 1500$ (red line) and $\omega_{pe} t = 2250$ (blue line) is shown.

4. CONVERGENCE

The density and momentum distribution are some of the lowest order criteria to check when modeling a collisionless shock. To assess the impact of our relatively limited simulation domain we compared the different 2D runs, finding that the limited box size has only a minor impact on the jump conditions and on the evolution of the filaments. Analyzing the 2D runs we find that a box with 250x7000 cells contains a shock with velocity $v_{sh} = 0.42c$, and a downstream to upstream density ratio of $n_d/n_u = 3.24$, while a box with twice the length, independent of the transverse size, more faithfully reproduces the analytic jump conditions. With $v_{sh} = 0.47c$ and a density jump of 3.12 it is in percent precision agreement with the analytic expectation for a relativistic gas $n_d/n_u = \gamma_{ad}/[\Gamma\gamma_{ad} - 1] + 1/[\Gamma(\gamma_{ad} - 1)]$, where γ_{ad} is the adiabatic index of the gas, which is 4/3 (3/2) for a 3D (2D) relativistic gas. This is also seen in the 3D case, where we find $v_{sh} = 0.27$ and $n_d/n_u = 4.62$, where analytically one expects $v_{sh} = 0.31$ and $n_d/n_u = 4.2$ (see figure 4). Because we launch the shock reflecting cold streaming particles on a wall it takes some time until a proper, thermalized downstream region is created. The electromagnetic fields at and near the shock interface have to

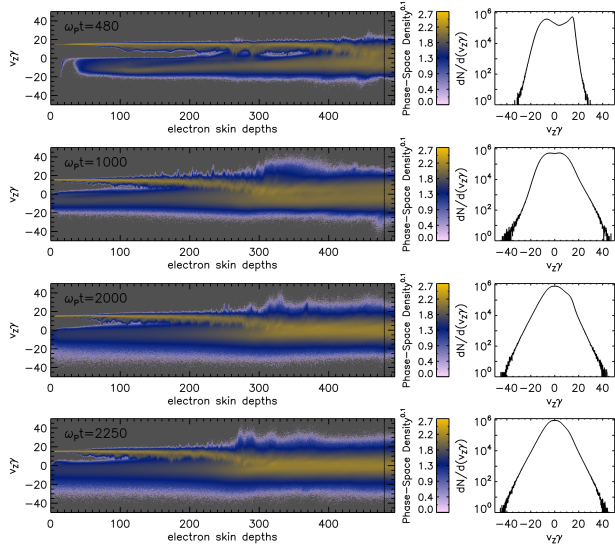


FIG. 5.— Evolution of the ions in phase space. The PDF is sampled to the right of the dotted line. Notice that it is only after $\omega_{pe}t \simeq 2000$ that the downstream part of the shock is completely thermalized and at rest. At earlier times the impact of the wall is still significant, with the return current of reflected particles apparent in the camel shaped pdf.

build up to a sufficient level to scatter the particles, and the shock interface has to be far enough away from the wall at the upper boundary, so that upstream particles are scattered by the fields and thermalize thoroughly before they possibly reach the wall. This convergence can be monitored by looking at the $v_z\gamma$ momentum near the wall. A camel shaped PDF signals that proper pressure support in the downstream region has still not been established. We find (see figure 5) that the simulation has to run to $\omega_{pe}t = 2000$ or $\omega_{pi}t = 500$ before a proper equilibrium is established, even though the proper jump conditions are already established at $\omega_{pe}t = 1000$ (see figure 4). Without the moving frame approach it would have required a box with at least 28000 cells in the streaming direction to properly establish and thermalize the shock.

5. CONCLUSIONS

In this Letter we have studied for the first time the long time behavior of a fully developed 3D collisionless ion-electron shock. We find that the development of the shock structure is similar to that of an electron-ion shock in a 2D model, but there are both qualitative and quantitative differences of importance when making quantitative predictions from shock models for observations. Apart from the dimensionality, which gives rise to different shock jump conditions, the extra degree of freedom changes the shock in a number of ways: 1) The current channels upstream of the shock become more stable. 2) Very strong parallel electric fields along the field lines are created at the shock interface giving a new and effective avenue for particle acceleration, as compared to 2D models. 3) The level of magnetic field energy is lower near the shock interface 4) A power-law tail in the PDF downstream of the shock emerges at late times. In agreement with theory the power-law index is shallower in the 3D shock (~ 2.2) compared to the 2D model (~ 2.5).

In Trier Frederiksen et al. (2010) it was found that the radiation emitted from the Weibel instability in 2D and 3D is qualitatively different, and analogously we expect that the differences presented here in the physical development of a 3D shock compared to a 2D shock will give rise to significant differences in the emitted radiation. This is a topic for future studies.

TH acknowledges support from the Danish Natural Science Research Council. Computer time was provided by the Danish Center for Scientific Computing (DCSC). It is a pleasure to thank J. T. Frederiksen, M. Medvedev, and Å. Nordlund for many valuable discussions and comments.

REFERENCES

- [PCCP] <http://comp.astro.ku.dk/Twiki/view/PicCodeComparison/WebHome>
- Bret, A., Firpo, M., & Deutsch, C. 2004, *Phys. Rev. E*, 70, 046401
- Chang, P., Spitkovsky, A., & Arons, J. 2008, *ApJ*, 674, 378
- Ergun, R. E., Andersson, L., Tao, J., Angelopoulos, V., Bonnell, J., McFadden, J. P., Larson, D. E., Eriksson, S., Johansson, T., Cully, C. M., Newman, D. N., Goldman, M. V., Roux, A., Lecontel, O., Glassmeier, K., & Baumjohann, W. 2009, *Physical Review Letters*, 102, 155002
- Ergun, R. E., Su, Y., Andersson, L., Carlson, C. W., McFadden, J. P., Mozer, F. S., Newman, D. L., Goldman, M. V., & Strangeway, R. J. 2001, *Physical Review Letters*, 87, 045003
- Frederiksen, J. T., Hededal, C. B., Haugbølle, T., & Nordlund, Å. 2004, *ApJ*, 608, L13
- Haugbølle, T. 2005, PhD thesis, Niels Bohr Institute [astro-ph/0510292]
- Hededal, C. 2005, PhD thesis, Niels Bohr Institute [astro-ph/0506559]
- Hededal, C. B., Haugbølle, T., Frederiksen, J. T., & Nordlund, Å. 2004, *ApJ*, 617, L107
- Hededal, C. B., & Nishikawa, K. 2005, *ApJ*, 623, L89
- Kato, T. N. 2007, *ApJ*, 668, 974
- Kazimura, Y., Sakai, J. I., Neubert, T., & Bulanov, S. V. 1998, *ApJ*, 498, L183+
- Keshet, U., Katz, B., Spitkovsky, A., & Waxman, E. 2009, *ApJ*, 693, L127
- Keshet, U., & Waxman, E. 2005, *Physical Review Letters*, 94, 111102
- Martins, S. F., Fonseca, R. A., Silva, L. O., & Mori, W. B. 2009, *ApJ*, 695, L189
- Medvedev, M. V., & Loeb, A. 1999, *ApJ*, 526, 697
- Nishikawa, K., Hardee, P., Richardson, G., Preece, R., Sol, H., & Fishman, G. J. 2003, *ApJ*, 595, 555
- Nishikawa, K., Niemiec, J., Hardee, P. E., Medvedev, M., Sol, H., Mizuno, Y., Zhang, B., Pohl, M., Oka, M., & Hartmann, D. H. 2009, *ApJ*, 698, L10
- Saito, S., & Sakai, J. 2004, *Physics of Plasmas*, 11, 859
- Schindler, K., Hesse, M., & Birn, J. 1988, *J. Geophys. Res.*, 93, 5547
- Shimada, N., & Hoshino, M. 2004, *Physics of Plasmas*, 11, 1840
- Silva, L. O. 2006, in *American Institute of Physics Conference Series*, Vol. 856, *Relativistic Jets: The Common Physics of AGN, Microquasars, and Gamma-Ray Bursts*, ed. P. A. Hughes & J. N. Bregman, 109–128
- Silva, L. O., Fonseca, R. A., Tonge, J. W., Dawson, J. M., Mori, W. B., & Medvedev, M. V. 2003, *ApJ*, 596, L121
- Sironi, L., & Spitkovsky, A. 2009, *ApJ*, 698, 1523
- Spitkovsky, A. 2005, in *American Institute of Physics Conference Series*, Vol. 801, *Astrophysical Sources of High Energy Particles and Radiation*, ed. T. Bulik, B. Rudak, & G. Madejski, 345–350 [astro-ph/0603211]
- Spitkovsky, A. 2008a, *ApJ*, 673, L39
- . 2008b, *ApJ*, 682, L5
- Trier Frederiksen, J., Haugboelle, T., Medvedev, M. V., & Nordlund, A. 2010, *ArXiv e-prints*
- Tzeng, K.-C., Mori, W. B., & Decker, C. D. 1996, *Phys. Rev. Lett.*, 76, 3332